

We are IntechOpen, the world's leading publisher of Open Access books Built by scientists, for scientists

6,900

Open access books available

186,000

International authors and editors

200M

Downloads

Our authors are among the

154

Countries delivered to

TOP 1%

most cited scientists

12.2%

Contributors from top 500 universities



WEB OF SCIENCE™

Selection of our books indexed in the Book Citation Index
in Web of Science™ Core Collection (BKCI)

Interested in publishing with us?
Contact book.department@intechopen.com

Numbers displayed above are based on latest data collected.
For more information visit www.intechopen.com



Heat Transfer Phenomena in Laminar Wavy Falling Films: Thermal Entry Length, Thermal-Capillary Metastable Structures, Thermal-Capillary Breakdown

Viacheslav V. Lel and Reinhold Kneer
*Institute of Heat and Mass Transfer, RWTH Aachen University,
 Germany*

1. Introduction

Liquid film flows are widely used in industrial applications and for example offer solutions for problems associated with the cooling of mechanical parts and electrical components where, for an optimum design of industrial devices, detailed knowledge about the different heat transfer phenomena in falling films is required. This chapter focuses on the three dominating aspects, such as

- formation and development of quasi-regular metastable structures within the residual layer between large waves;
- thermal-capillary breakdown of laminar-wavy falling film and
- thermal entry length.

1.1 Thermal-capillary metastable structures and thermal-capillary breakdown

Typically, a decrease in film thickness leads to an increase of the heat and mass transfer. However, very thin films are prone to flow breakdowns, which cause dry spot formation. In extreme cases, the appearance of dry spots and, as a consequence, a drastic reduction of the heat transfer at the solid liquid interface may lead to thermal destruction of the carrier surface.

There are several mechanisms leading to the appearance of dry spots: evaporation of liquid within the residual layer, i.e. between large waves, film separation due to interaction with the surrounding gas flow, a boiling crisis in the liquid film, a thermo-diffusive and thermo-capillary breakdown of the film due to concentration gradients or a temperature gradient on the film surface. For the thermo-capillary caused flow of fluid near the surface in falling films a detailed understanding is missing so far.

Some insight into thermo-capillary phenomena have been provided by the experimental study of (Kabov & Chinnov, 1998 and Kabov et al., 2001). These studies comprised investigations of slightly inclined heating surfaces in the small Reynolds number range where inertia can be neglected and as a consequence the free surface developed a two-dimensional stationary bump above the heater due to thermo-capillary Marangoni effects only. At a critical value of the heat flux from the heater to the liquid the bump developed an

instability in the transverse direction that took the form of rivulets at the downstream edge of the bump. The first experiments relative to Marangoni instabilities were shown in the work by (Slattery & Stuckey, 1932) by draining a liquid film. Later, (Ludviksson & Lightfoot, 1968) formulated a hydrodynamic stability analysis of the problem, presented in (Slattery & Stuckey, 1932).

Jet formation in laminar-wavy flow was visualised recently by (Chinnov & Kabov, 2003). In this case the falling film is wavy through the hydrodynamic instability. Kalliadasis and co-workers (see for example Trevelyan & Kalliadasis, 2004; Scheid et al., 2005; Ruyer-Quil et al., 2005) in their theoretical works showed that at small Reynolds numbers increasing the Marangoni number leads to larger amplitudes and spreads of the solitary pulses since the two instability modes (Kapiza and Marangoni) reinforce each other. On the other hand, in the region of large Reynolds numbers the destabilising Marangoni forces are weaker than the dominant inertia forces. Investigations (Pavlenko & LeI, 1997; Pavlenko et al., 2002) also revealed the presence of regular structures in the form of alternating jets and dry spots in the flow of saturated laminar-wavy liquid films with intense evaporation or boiling.

For the study of thermo-capillary phenomena in falling liquid films information about the surface temperature and the film thickness field is needed. The surface temperature distribution can only be found using non-invasive techniques. (Yüksel & Schlünder, 1988) used a pyrometer for the investigation of the temperature of the falling film's surface. This point technique requires a complex mechanical periphery for the determination of a surface temperature field.

This can be achieved more easily using a focal-plane-array IR camera (Klein et al., 2005). This approach has been pursued in this study. In addition, the camera used here attains a frame rate of up to 2,000 frames per second depending on the size of the array (Al-Sibai et al., 2003). Therefore, the surface temperature distribution of the entire film within the test section can be measured at the same time with a high temporal and spatial resolution. The disadvantage of the camera is that the detector chip requires a more complicated calibration procedure than a single point pyrometer and thus the pyrometer is better suited if absolute temperature measurements are required.

The thickness distribution of three-dimensional waves in laminar falling films was investigated by (Adomeit & Renz, 2000) using a fluorescence technique. A small amount of sodium-fluorescein ($C_{20}H_{10}Na_2O_5$) was added to the film as a fluorescent tracer. The tracer irradiates a bright orange light when exposed to UV-light. The emitted fluorescent light was recorded by a CCD camera equipped with a UV-filter and the brightness distribution was converted into the film thickness field using a calibration procedure. The error of this technique is approximately 0.02 mm, while the film thickness lies in the range of 0.1 up to 2.0 mm. Its disadvantage is the complicated calibration procedure and the dependence of the emitted light on the temperature. This can be avoided when studying falling films using excited waves (Alekseenko et al., 1994). In this case point thickness measurements can be transformed into field data, because the consecutive waves arise in the same places.

1.2 Thermal entry length of falling films

Only few publications relating to the thermal entry length of falling films are available. (Mitrovic, 1988) and (Nakoryakov & Grigorijewa, 1980) determine the thermal entry length of smooth laminar falling films defining the thermal entry length L_δ as the average distance between the beginning of a heated plate and the point where the thermal boundary layer

arrives at the film surface. This approach was also adopted here. The results of (Mitrovic, 1988) and (Nakoryakov & Grigorijewa, 1980) yield a similar correlation for L_δ :

$$L_\delta = cRe_0^{\frac{4}{3}}Pr_0\left(\frac{v^2}{g}\right)^{\frac{1}{3}} \quad (1)$$

differing only in the numerical value of the constant c . (Mitrovic, 1988) found a value of $c = 0.0974$, whereas in (Nakoryakov & Grigorijewa, 1980) has a value of $c = 0.06$. Here the following symbols are used $Pr = \nu/a$ (Prandtl number), $Re = \dot{V}/\nu B$ (Reynolds number), \dot{V}/B (volume flow rate per test section width), a (thermal diffusivity), ν (kinematic viscosity), g (gravitational acceleration).

When comparing laminar-wavy film flow with smooth laminar film flow, the influence of the Reynolds number could change since an influence of the waves can be assumed. Also the film thickness in the residual layer of laminar wavy films is smaller than the one of laminar-waveless films at the same Reynolds number.

Furthermore, the solutions derived by (Mitrovic, 1988) and (Nakoryakov & Grigorijewa, 1980) presume constant material properties which do not comply with changing temperatures in the flow, since due to the heating of the fluid the Prandtl numbers at inflow (Pr_0) and wall (Pr_w) temperature are different. With the temperature increase of the fluid its Prandtl number decreases and thereby the thermal entry length decreases as well. Thus, the ratio Pr_0/Pr_w should be added to the thermal entry length correlation.

The thermal entry length can also be referred to as the length L_α between the beginning of the heated section and the point from which on the heat transfer coefficient α remains constant. According to (Mitrovic, 1988), the ratio L_α/L_δ is about 2.2 for laminar flow. This means that the heat transfer coefficient takes much longer to reach a constant level than the thermal boundary layer to grow up to the film thickness. The time averaged ratio L_α/L_δ should be similar in laminar-wavy flow. Unfortunately, the local heat transfer coefficient could not be measured in the present set-up and therefore this value could not be confirmed.

Infrared thermography makes it possible to measure the surface temperature of the film flow without disturbing it, provided the film is opaque (Kabov et al., 1995). In (Kabov et al., 1996) an IR technique is used to determine the thermal entry length for a smooth film and it is qualitative shown that this length decreases with the heat flux because of Marangoni convection in the direction opposite to the main flow. Presented in Chap. 2.4 experimental data of the thermal entry length of laminar wavy falling films were obtained by means of infrared thermography too.

2. Experimental examination

2.1 Experimental setup

The closed-loop test facility is shown in Fig. 1. Silicone fluid is supplied from a liquid distributor through an adjustable gap onto the 150 mm wide test section. The test section consists of a vertical polyvinylchloride plate with a copper plate (130 x 70 mm² or 130 x 140 mm²) mounted in the hydrodynamically established region 330 mm downstream of the distribution gap. At the end of the test section the liquid film flows into a reservoir. The fluid is circulated by an adjustable piston pump. The flow rate is measured by a positive displacement flow meter. The experiments were carried out in a Reynolds number range

between 2 and 39. The variation of Reynolds numbers was limited by the pump capacity. The entrance temperature of the liquid T_1 is checked by a thermocouple in the liquid distributor and is kept constant using a heat exchanger in the lower reservoir. Also, for safety reasons the liquid temperature T_2 is monitored with a thermocouple at a vertical position parallel to the measurement area. In order to avoid disturbances of the film flow this thermocouple is displaced sideways. The temperatures T_4 within the heater is measured at eight measurement points at distances of 6 and 10 mm from the surface. To excite regular waves on the liquid surface a loudspeaker above the upper reservoir is used.

The heat flux is regulated by adjusting the voltage supplied to heating cartridges in the copper plate. The average heat flux \dot{q}'' in the experiments was set between 0 and $3.1 \times 10^4 \text{ W m}^{-2}$. An error less than 3% was assessed taking into account that heat losses through the isolation can be neglected. Silicone oils (Polydimethylsiloxane [DMS-T]) of different viscosity were used as test fluids to allow for a variation of the Prandtl number Pr between 57 and 167. The material properties of the different liquids are presented in Table 1.

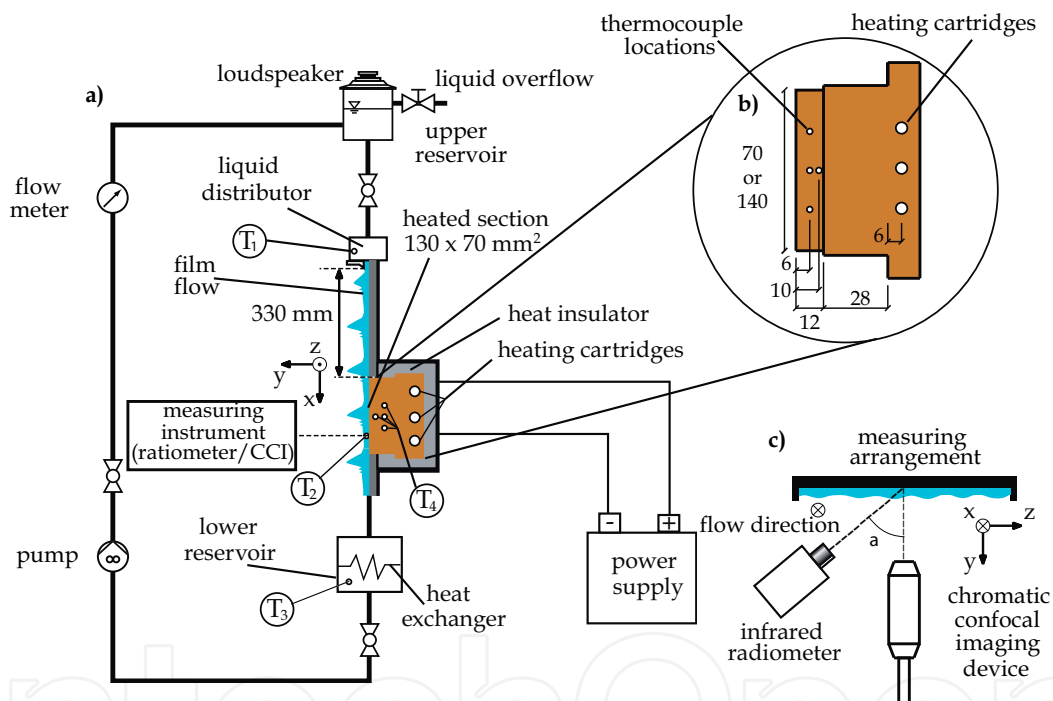


Fig. 1. a) Sketch of the test facility, b) heater, c) position of the measurement devices (Lel et al., 2008)

For description of the kinematic viscosity of DMS-T11 up to 100°C the Vogel-Fulcher-Tammann-equation was used, (Dietze, personal communication).

$$\eta[\text{Pa}\cdot\text{s}] = \frac{\exp(-3.748 + \frac{1848.1}{18 + T[\text{K}]})}{1000} \quad (2a)$$

For the dynamic viscosity of DMS-T05 and DMS-T12 the linear dependencies were used:

$$\nu \left[\frac{\text{m}^2}{\text{s}} \right] = 6.62 \cdot 10^{-6} \left[\frac{\text{m}^2}{\text{s}} \right] - 7.37 \cdot 10^{-8} \left[\frac{\text{m}^2}{\text{s}^\circ\text{C}} \right] \cdot T [^\circ\text{C}] \quad \text{for DMS-T05} \quad (2b)$$

$$\nu \left[\frac{\text{m}^2}{\text{s}} \right] = 23.01 \cdot 10^{-6} \left[\frac{\text{m}^2}{\text{s}} \right] - 26.04 \cdot 10^{-8} \left[\frac{\text{m}^2}{\text{s}^\circ\text{C}} \right] \cdot T [^\circ\text{C}] \quad \text{for DMS-T12} \quad (2c)$$

Experiments have been carried out at atmospheric pressure and ambient temperature.

	DMS-T05	DMS-T11	DMS-T12
ρ (kg m ⁻³)	918	938	950
σ (N m ⁻¹)	0.0197	0.0201	0.0206
$d\sigma/dT$ (N K ⁻¹ m ⁻¹) (10 ⁻⁵)	-6.7	-6.7	-6.7
c_p (J kg ⁻¹ K ⁻¹)	1,546	1,546	1,546
λ (W m ⁻¹ K ⁻¹)	0.119	0.136	0.145
ρ_{IR} (9.0 < λ < 9.5 μm) (-)	0.049	0.052	0.055
$Pr = \nu/a$ (-)	57	93	167
$Ka = (\sigma^3 \rho)/(g \eta^4)$ (-)	1,935,716	176,435	14,037

Table 1. Physical properties for silicone fluids Polydimethylsiloxane (DMS-T) at T = 25°C (Lel et al., 2007a)

2.2 Infrared radiometer

For the time-resolved recording of the temperature field an IR-camera CEDIP JADE 3 LW with a 320 x 240 HgCdTe focal-plane-array has been used. The camera operates in the long wavelength region between 7.7 and 9.5 μm . Using an additional filter which blocks all radiation below a wavelength of 9.0 μm , it is possible to measure the temperature in a very thin layer of the surface of the film (Al-Sibai et al., 2003). According to measurements conducted at the Institute for Organic Chemistry at RWTH Aachen University (Fig. 2a) the average absorption coefficient of the fluids at wavelengths between 9.0 and 9.5 μm is between $\alpha_{\text{IR}} = 3 \times 10^5$ and $\alpha_{\text{IR}} = 4 \times 10^5 \text{ m}^{-1}$. Average reflection coefficients in the relevant range of wavelengths are included in Table 1.

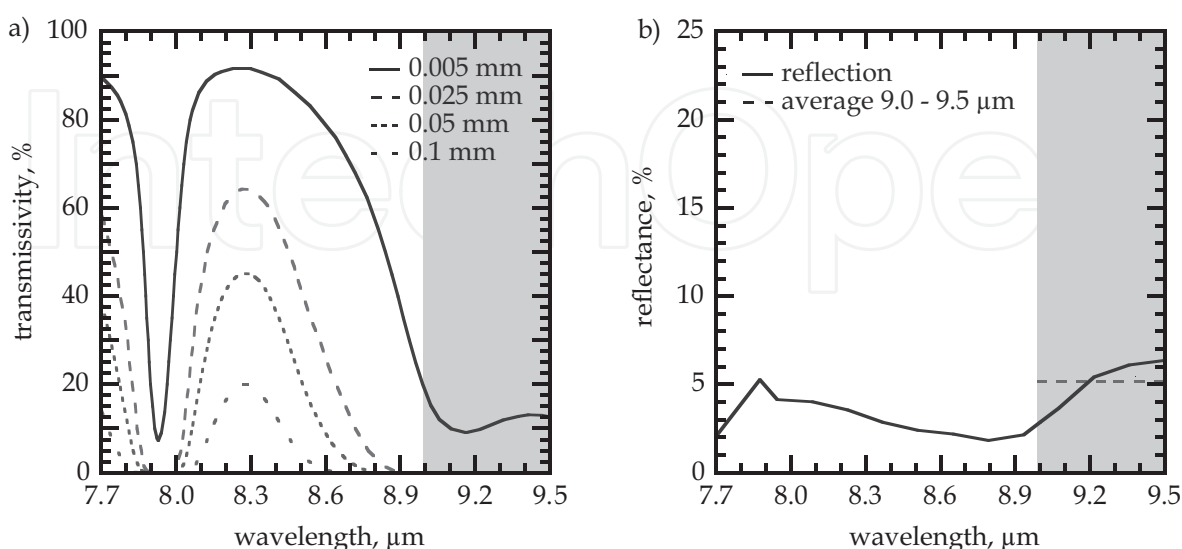


Fig. 2. Optical properties of the silicone fluid DMS-T11. a) Spectral transmissivity for layers of different thicknesses (Bettray, 2002), b) spectral reflectance (Mayerlen & Tacke, 2002)

Knowing the absorption coefficient allows to estimate that 99% of the radiation is absorbed in a thin layer at the surface, having a thickness between 10 and 15 μm . The spectral reflectance of the silicone fluid was measured at another research institute (Mayerlen & Tacke, 2002), whose results are presented in Fig. 2b. The average reflection coefficient in the range of wavelengths between 9.0 and 9.5 μm is $\rho_{\text{IR}} = 0.052$.

The sensitivity (NETD) of this camera is about 25 mK. The integration time of the IR-camera varies depending on the range of working temperatures. For the given range of temperatures it was set to 500 μs . For a given set of parameters the film flow was recorded over period of 5 s at a frame rate of 200 Hz. The surface area recorded was 70 x 108 mm or 140 x 216 mm. This is equivalent to a resolution of 0.33 x 0.33 mm^2 or 0.66 x 0.66 mm^2 per pixel accordingly.

2.3 Chromatic confocal imaging

The film thickness was measured using a chromatic confocal imaging (CCI) technique (STIL CHR-450, see Cohen-Sabban et al., 2001). Its measuring principle is shown in Fig. 3a. Light from a polychromatic source passes through a semi-transparent mirror. Due to chromatic aberration the lens splits the white light into a continuum of monochromatic images with focal points at different distances. The measuring range (the distance between the focal points of the shortest and the longest used wavelength) is 2.7 mm. The light is reflected from the measured surface and conducted to the spectrometer. A spatial filter eliminates the wavelengths which are not in focus on the measured surface. The wavelength for which the spectrometer detects the highest intensity is the one in focus on the object. By means of a calibration curve this wavelength is converted to a position in the measuring range. This technique has been extended in (Lel et al., 2005) for measuring the thickness of falling liquid films for adiabatic fluid flow. The film surface reflection signal (the wavelength λ_{FS} , see Fig. 3b) is about ten times weaker than the one from the wall surface (the wavelength λ_{WS} , see Fig. 3b) and thus is often equal to the noise level, when the film surface is not parallel to the wall. Therefore the film thickness measurement refers only to the signal reflected from the wall. For the determination of the film thickness δ_r (Fig. 3b) the wall position y_3 has to be known before the start of the film thickness measurement. During the measurements only position y_2 is obtained. Then:

$$\delta_w = y_2 - y_3 \quad (3)$$

and

$$\delta_r = \frac{\delta_w n(\lambda_{\text{WS}})}{n(\lambda_{\text{WS}}) - 1} \quad (4)$$

Where $n(\lambda_{\text{WS}})$ is the refractive index for the wavelength λ_{WS} , reflected at the wall surfaces.

In the case of heat transfer between surface and film, the heated copper plate expands in an uncontrolled manner and consequently the original position y_3 is displaced to position y_{3^*} . To determine y_{3^*} , the signal from the spectrometer, which is obtained at the times, when film and wall surfaces are parallel (usually in the residual layer between large waves), is analysed for two maxima λ_{FS} and λ_{WS} and the corresponding positions y_1 and y_2 within the measuring range of the optical sensor are calculated, Fig. 3b. The real film thickness and the exact position of the wall y_{3^*} then can be evaluated using the optical law:

$$\delta_r = \delta_{opt} n(\lambda_{WS}), \tag{5}$$

and therefore

$$y_{3^*} = (y_2 - y_1) n(\lambda_{WS}) + y_1, \tag{6}$$

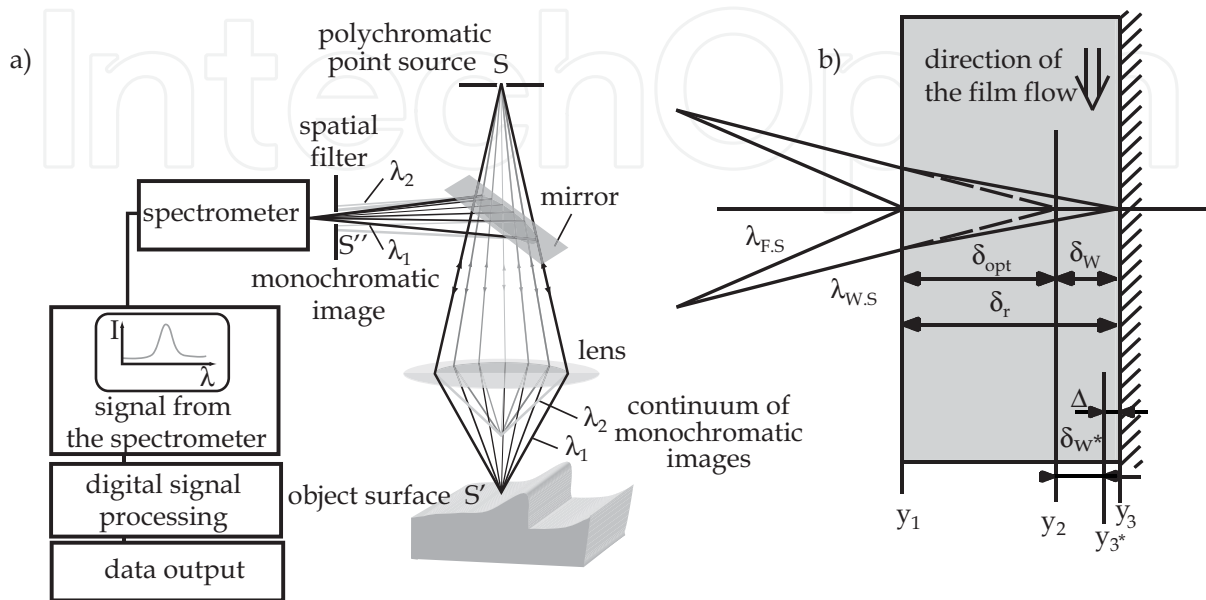


Fig. 3. a) Chromatic confocal imaging principle (Lel et al., 2005), b) light beam path through a falling film (Lel et al., 2008)

For the determination of δ_W , the position y_{3^*} has to be inserted into Eq. (3) instead of y_3 . The procedure of refractive index $n(\lambda_{WS})$ determination is shown in Fig. 4. From the position within measuring range y_2 the wavelength λ_{WS} is determined and converted to the refractive index with the help of the dependencies shown in Fig. 4b.

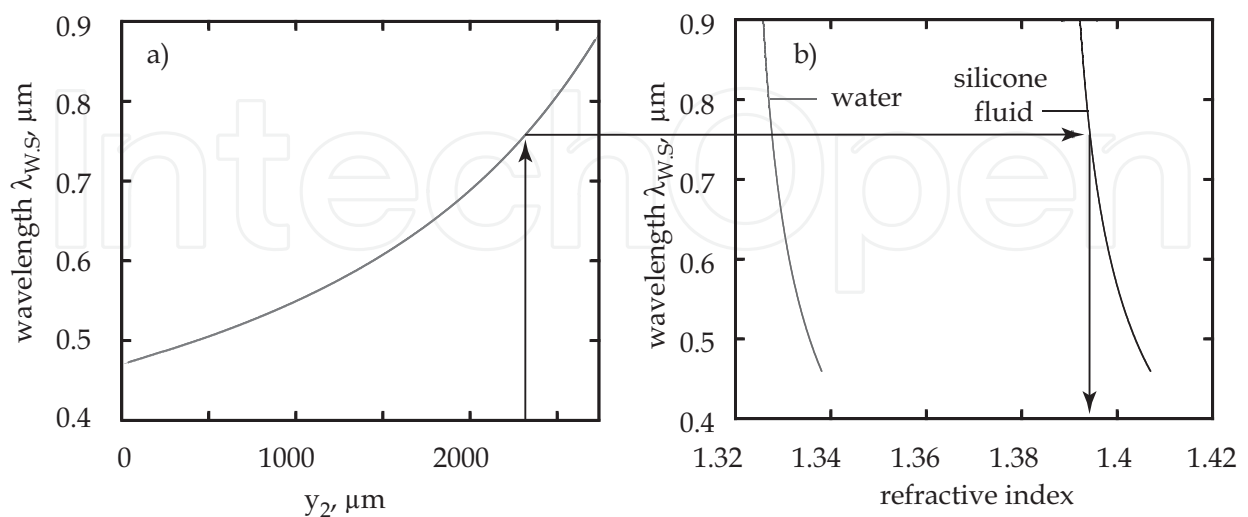


Fig. 4. The procedure of refractive index determination. a) Dependence between wavelength λ_{WS} and position within measuring range, b) Dependence between wavelength λ_{WS} and refractive index for silicone fluid and water (Lel et al., 2008)

2.4 Thermal entry length evaluation

The procedure of evaluating the thermal entry length from the infrared frames is shown on the basis of the example in Fig. 5. There the nondimensional temperature of the film surface according to Mitrović (1988) is shown in Fig. 5.b):

$$\Theta = \frac{T_w - T}{T_w - T_0} \quad (7)$$

Two horizontal stripes, one at the top and one at the bottom of the heated section can be seen (on the left and right sides in the image). The respective edges are shown as start and end markers. These stripes are spanned over the film so that the beginning and the end of the heated surface can be determined in the infrared recordings. The distance between both corresponds to the length of the heated section.

To determine the entry length, a slice A-A with a width of three pixels in the centre of the images was investigated. This procedure allows to average out faulty pixels within the detector array and to reduce noise from the pixels. Within the slice the inflow temperature for the film was identified by averaging over the first 10 pixels over all frames of each film.

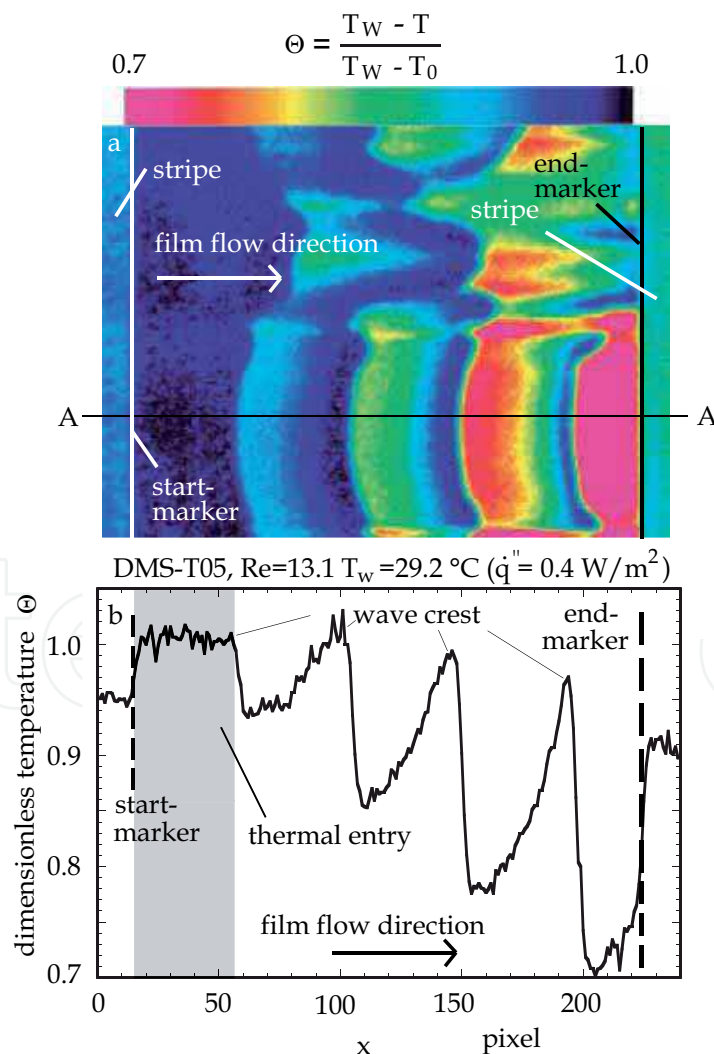


Fig. 5a), 5b) Nondimensional temperature Θ at the film surface (Lel et al., 2007b)

The graph of the nondimensional temperature distribution of the slice A-A, which is marked in Fig. 5a), can be seen in Fig. 5b). Clearly visible are the two stripes that are spanned over the film (the start and the end marker) in the beginning and in the end of the graph. The inflow temperature can be distinguished as the plateau at $\Theta = 1$, which varies in length over time. This plateau is also the thermal inflow length as it is defined for the present work. The noise in the data is smaller than the difference to the threshold value, $\Delta\Theta < 0.01$, which is equivalent to about 0.1 K for the example shown.

The first steep decline in the nondimensional temperature marks the front of a cool wave crest. Further downstream the residual layer is already heated up. In the direction of the flow the residual layer becomes cooler again until another wave crest is reached. This cooling is probably caused by the increasing thickness of the film. Measurements of the film thickness endorse this assumption. The second wave crest is again at inflow temperature. From the next wave crest on, an increase in the temperature can be determined.

At the certain momentary residual layer thickness the thermal boundary layer can grow to film thickness before a wave appears. In this case the current entry length is smaller than the distance between two large waves.

3. Regular structures within the residual layer

In this part the results of the visualization of the regular structures within the residual layer by means of infrared thermography and CCI technique are presented.

Fig. 6 shows a typical IR picture of quasi-regular metastable structures within the residual layer between large waves of laminar-wavy falling films. These structures propagate in flow direction (x-direction), whereas in cross direction (y-direction) the alternating nature of the structures, showing low and high surface temperatures can be determined. The distance between the two hot stripes is shown in Fig. 6 as Λ . As shown in a recent publication (Lel et al., 2007a), no dependence of the mean distance Λ between two hot stripes on the liquid flow rate has been found. This result differs from the conclusion of (Kabov et al., 2004). However the analysis of experimental data of (Kabov et al., 2004) shows, that almost all data for laminar-wavy films have same order of magnitude as the ones of (Lel et al., 2007a). Only the data for very low Reynolds Number (near to case of purely laminar film) have different values of transverse sizes of regular structures Λ .

There are supposedly two different mechanisms causing the development of regular structures. The first mechanism is the development of a large bump, whose instability then leads to the regular structures, with the wavelength being a function of Reynolds number. This phenomenon has been described in detail by Kabov and co-workers (see for example, (Kabov & Chinnov, 1998) and (Kabov et al., 2004)). The second case relates to the information of regular structures at the horizontal intersection points of larger, parabolic shaped wave fronts. The distance between these points was found (Lel et al., 2007a) to be in the same order as the critical length of the Rayleigh-Taylor instability and independent of the Reynolds number.

The stripes of high surface temperatures lie behind the intersection of the parabola-shaped waves and the temperature difference between the areas with the high and low temperatures grow until the arrival of the next wave front. The temporal evolution of the regular structure's "head" between two parabola-shaped waves is shown in Fig. 6b. From this series it can be seen, that until a time of 0.025 s, the top of the hot stripes (A) has no pronounced characteristic. From time 0.025 to 0.05 s the "head" of the regular structures rounds (B). Later it transforms to the mushroom form (C).

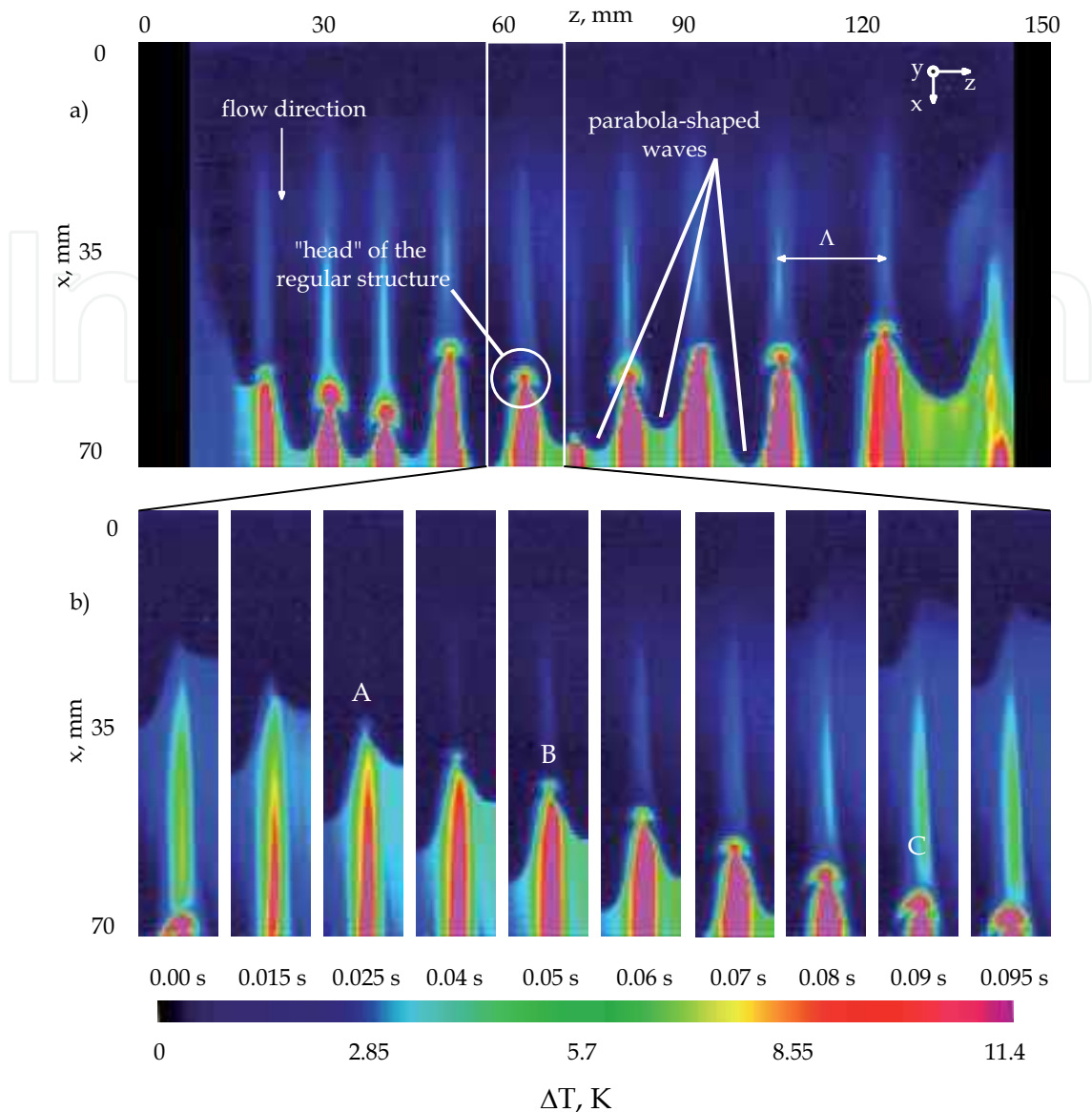


Fig. 6. a) Typical IR picture of quasi-regular metastable structures within the residual layer between large waves of laminar-wavy falling films, b) temporal evolution of the regular structure's "head" between two large parabola-shaped waves (zone marked in a), $Re = 15$, $\dot{q}'' = 2.2 \times 10^4 \text{ W/m}^2$ (Lel et al., 2008)

The structure's "head" effect could be explained through interference of waves at the point of intersection of two large parabola-shaped waves. The visualisation of falling films in the work of (Alekseenko et al., 1994) and (Scheid et al., 2006) shows, that capillary waves in front of large waves generate an interference pattern. Also from a recent work by (Lel et al., 2005) has become clear, that the point with the minimal film thickness is always found directly in front of large waves. Now, if interference effects exist in the area of intersection of two large parabola-shaped waves, then these effects are strongest directly in front of the large waves and their intersections. Thus, close to the position of minimum film thickness, maximum film thickness gradients and the temperature gradients have to be expected. There, Marangoni's forces and the forces, induced by surface curvature (Laplace pressure), exhibit maximum values.

The effect of the “mushroom form” is not completely clear. Probably in the spanwise direction (z-direction) only the viscous force is a counterforce to the Marangoni force and the force, inducted by surface curvature. In contrast to this, in flow direction (x-direction) the influence of gravitational and inertial forces could play a certain role. Therefore the “heads” of the regular structures change their form from round (B) to the mushroom (C).

Fig. 7 and Fig. 8 show some results of the visualisation of quasi-regular metastable structures within the residual layer between large waves of laminar-wavy falling films at Reynolds numbers of approximately $Re = 12$ and 18 as a function of heat flux. In the first rows, IR pictures of the surface are presented. The measurements without heat flux show a uniform surface temperature (upper Fig. 7a.1). In the lower Fig. 7a.1 and in Fig. 8a.1 IR pictures taken without black shielding are shown. These allow obtaining the information about the wave front shapes from reflection of the ambience radiation. This information was used for the film surface imaging, see (Lel et al., 2008).

In the second row of Fig. 7 and Fig. 8 the film thickness fields are presented. In the third row film thickness and surface temperature profiles in the residual layer (directly in front of the large waves) as a function of the horizontal position are shown. At the positions in the z direction, where intersections of the parabola-shaped waves are located, the local film thickness of the residual layer has a minimum in both cases. At the same time a temperature distribution emerges whose extrema are distributed inversely. The differences between maxima and minima of both, film thickness and temperature distribution, increase in parallel with increasing heat flux [column (a)-(c)]. This observation confirms the assumption of the thermo-capillary nature of structures within the residual layer between large waves. Probably the nonuniformity of the surface temperature leads to a nonuniformity of surface tension and as a consequence there is some mass transfer in z direction. This development can be seen more clearly on the right hand side of the test section where the positions of the parabola-shaped waves were more stable. Here, even the small stripes of lower temperatures in the middle of the hot zones can be associated with small crests in the residual layer (Fig. 7b zone A).

The spatially resolved averaged maximum, mean and residual layer film thickness are shown in the fourth row of Fig. 7 and Fig. 8. It can be seen from the pictures a.4 in both figures that the mean film thickness correlates very well with the Nusselt film thickness for laminar flows. However, there is some uneven distribution in the z direction possibly concerned with the external excitation of the film. With increasing heat flux there is a decrease of the mean film thickness. On the one hand this could be explained by the reduction of viscosity with increasing temperature, on the other hand cross flow into the large waves and their acceleration could take place. In the position where the parabola-shaped waves were more stable (right hand side of Fig. 7), the amplitude of the mean film thickness distribution rises with an increase of the specific heat transfer, too. The maximum and residual layer thickness decrease with increasing of the heat flux. The distribution of the former becomes more scattered.

Further analysis of the film thickness fields of Fig. 7 and the temperature as a function of time at the same measurement positions yields the corresponding flow wise profiles of film thickness and surface temperature at different horizontal positions (from the middle of large waves – row one, to the middle of the hot regular structures – row four) and heat fluxes (from the heat flux equal to zero – column one, to the heat flux equal to $2.2 \times 10^4 \text{ W/m}^2$), which are presented in Fig. 9. To ease orientation cut-outs from the film thickness fields of Fig. 7 are presented in each picture and the horizontal position is indicated by a vertical line.

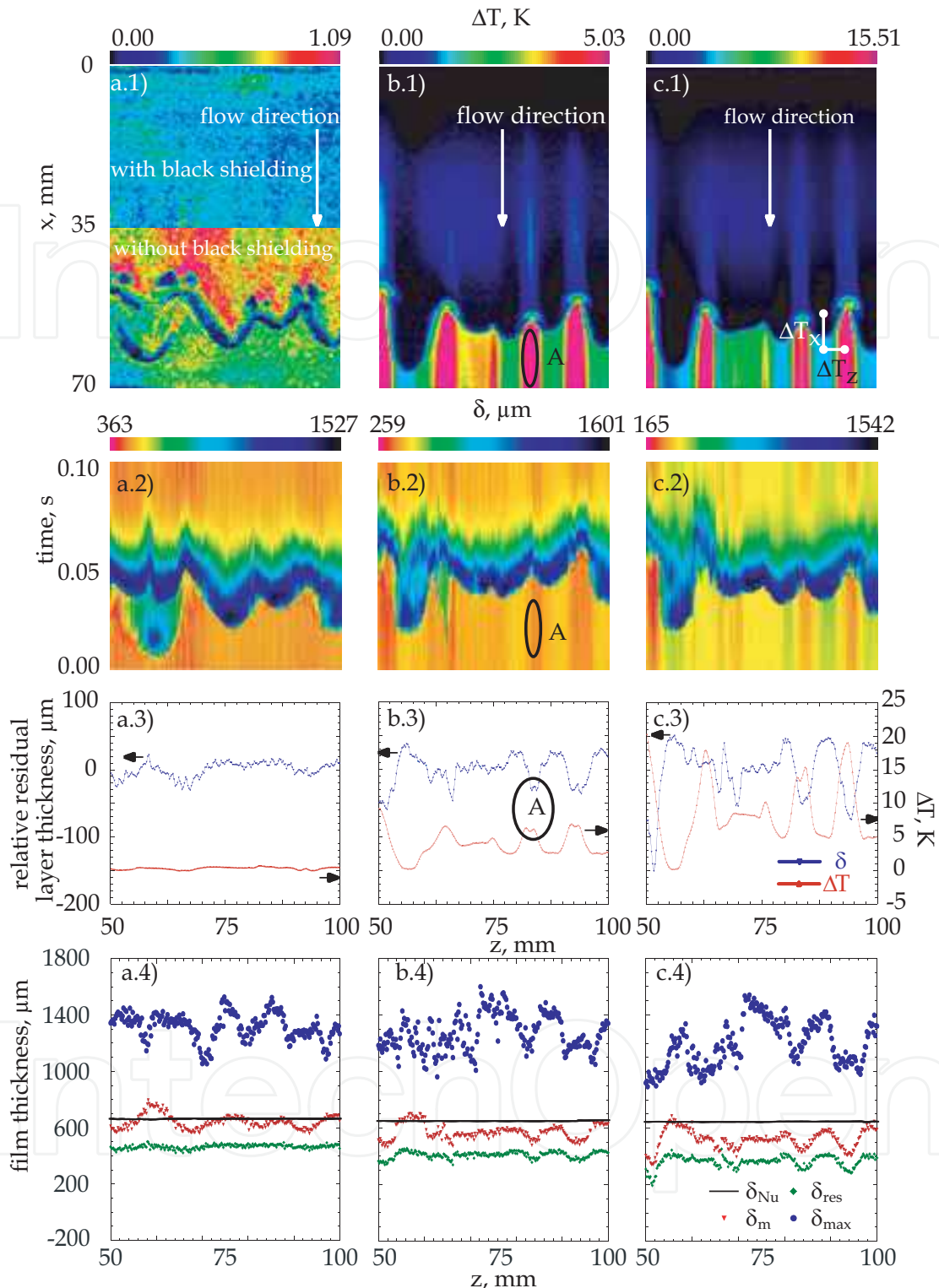


Fig. 7. Regular metastable structures within the residual layer. a) $Re = 12.0$, $\dot{q}'' = 0 \text{ W/m}^2$, b) $Re = 11.7$, $\dot{q}'' = 1.22 \times 10^4 \text{ W/m}^2$, c) $Re = 12.0$, $\dot{q}'' = 2.22 \times 10^4 \text{ W/m}^2$, 1) surface temperature field, IR picture, linear scale, 2) film thickness field, logarithmic scale, 3) film thickness and temperature profile in the residual layer 2 mm ahead of the large waves' front, 4) maximum (δ_{\max}), mean (δ_m), residual layer (δ_{res}) and Nusselt film thickness (δ_{Nu}), A: zone of double structure. (Lel et al., 2008)

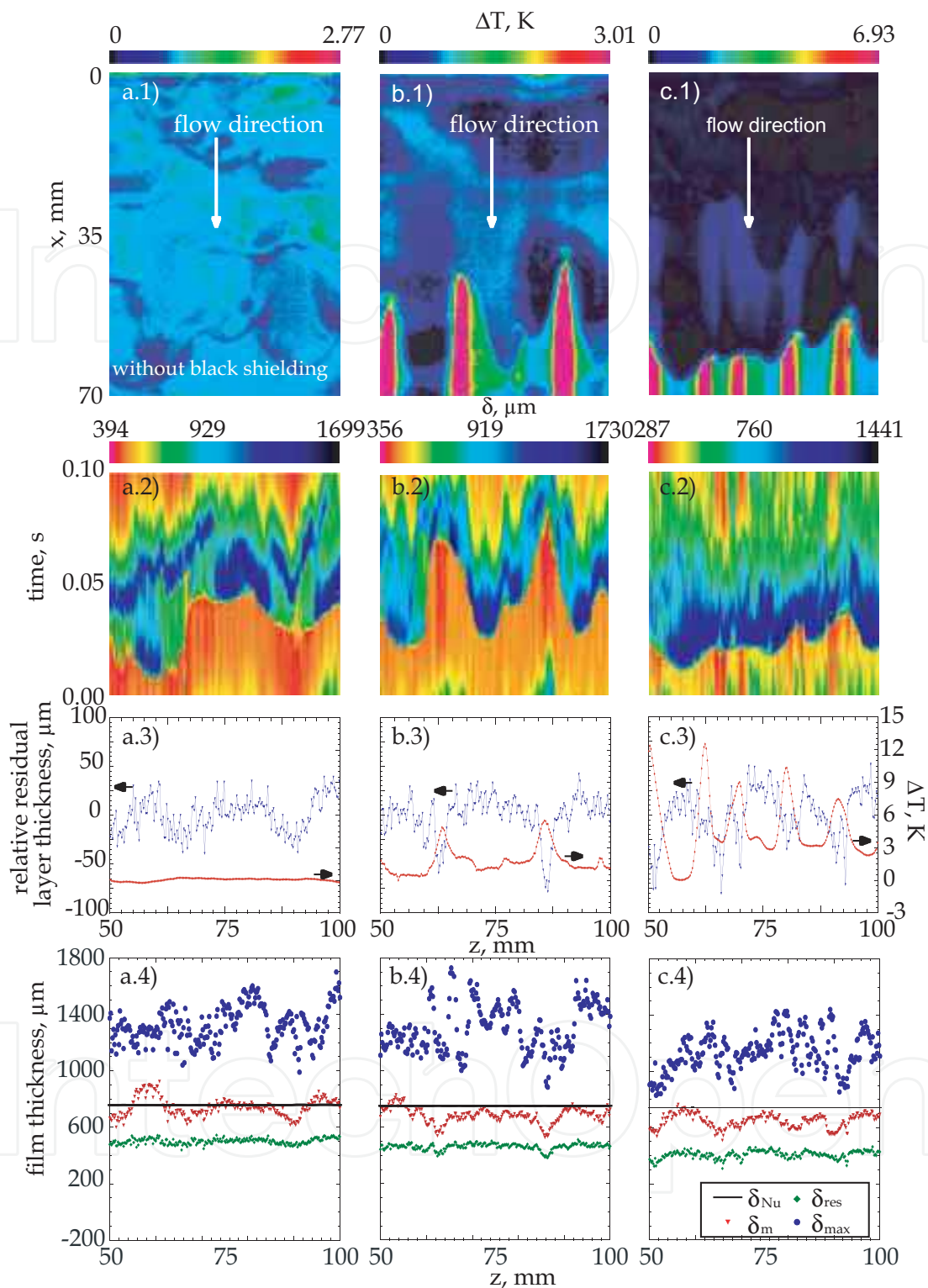


Fig. 8. Regular, metastable structures within the residual layer. a) $Re = 17.9$, $\dot{q}'' = 0 \text{ W/m}^2$, b) $Re = 18.0$, $\dot{q}'' = 1.04 \times 10^4 \text{ W/m}^2$, c) $Re = 18.0$, $\dot{q}'' = 2.23 \times 10^4 \text{ W/m}^2$, 1) surface temperature field, IR picture, linear scale, 2) film thickness field, logarithmic scale, 3) film thickness and temperature profile in the residual layer 2 mm ahead of the large waves' front, 4) maximum (δ_{\max}), mean (δ_m), residual layer (δ_{res}) and Nusselt film thickness (δ_{Nu}). (Lel et al., 2008)

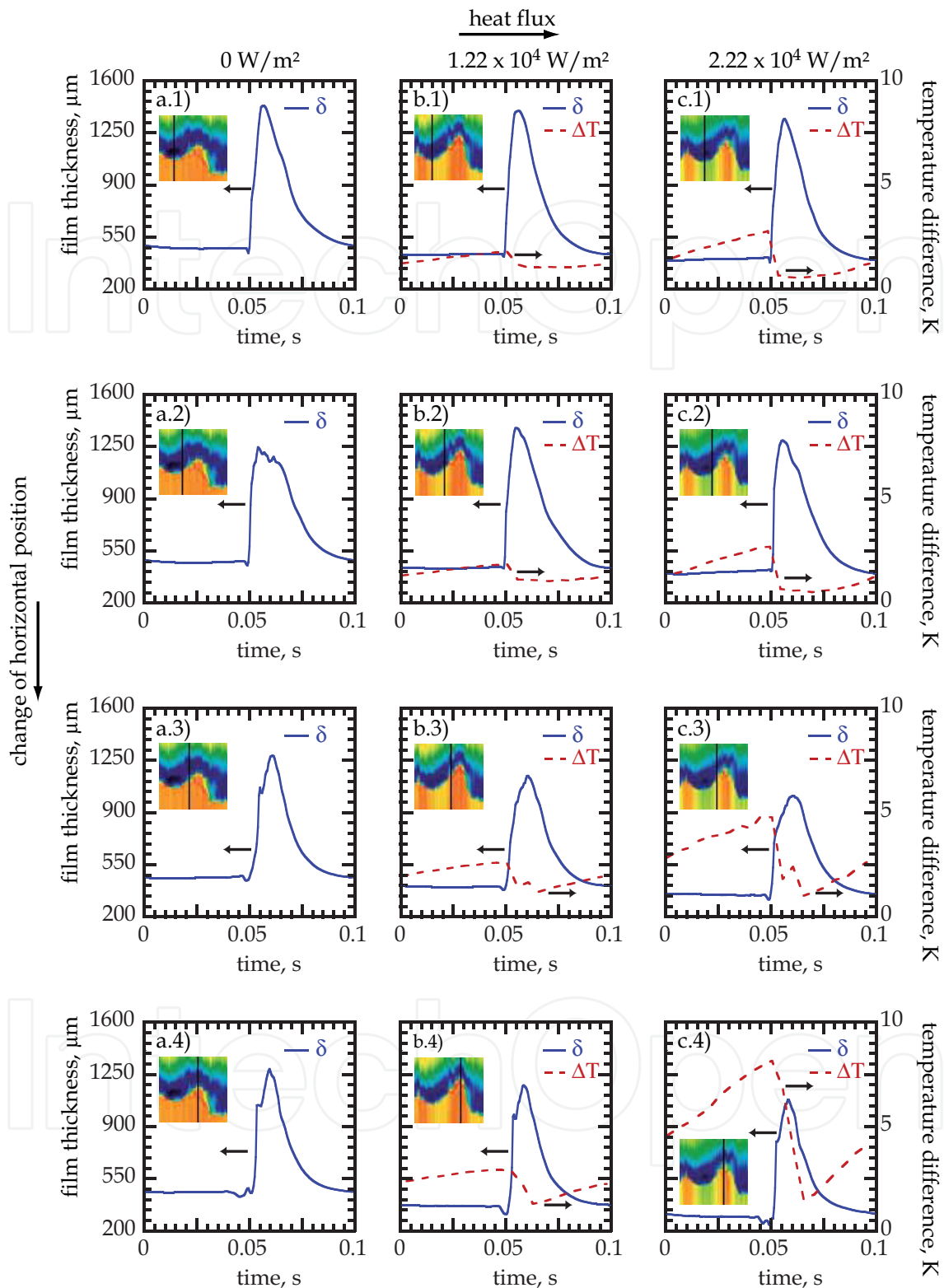


Fig. 9. The film thickness and the temperature profiles in the flow direction as a function of horizontal position and heat flux. a) $Re = 12.0$, $\dot{q}'' = 0 \text{ W/m}^2$, b) $Re = 11.7$, $\dot{q}'' = 1.22 \times 10^4 \text{ W/m}^2$, c) $Re = 12.0$, $\dot{q}'' = 2.22 \times 10^4 \text{ W/m}^2$, 1) in the middle of the large waves, 2) at the side of the large waves, 3) at the side of the hot regular structures, 4) in the middle of the hot regular structures. (Lel et al., 2008)

It can be seen that the difference between maximum and minimum temperatures increases, with increasing heat flux as well as with a change of the horizontal position from the middle of large waves to the middle of the hot regular structures.

In Fig. 10 the non-dimensional film thickness as a function of the heat flux is presented. The different symbols indicate different Reynolds numbers. Open symbols refer to a non-dimensionalisation via the Nusselt film thickness at the inflow temperature, filled symbols indicate the usage of the local temperature. It can be seen that the film thickness decreases with an increase of the heat flux. This can be explained by the decrease in fluid viscosity. However, in this case the ratio of mean film thickness to the Nusselt film thickness based on the local temperature $\delta_m/\delta_{Nu,local}$ should be independent from the heat flux, which obviously is not the case. It can be seen that the non-dimensional film thickness also decreases with increasing heat flux for all Reynolds numbers. Where the local Nusselt film thickness is calculated as:

$$\delta_{Nu,local} = \left(\frac{3\dot{V}}{Wg\nu(T_{loc})} \right)^{\frac{1}{3}} \tag{8}$$

where W is the width of test section.

The local temperature can be calculated from the equation:

$$T_{loc} = T_{in} + \frac{\dot{q}''WL}{\rho\dot{V}c_p} \tag{9}$$

where L is the distance between the beginning of the heated section and the measuring point, T_{loc} is the local fluid temperature at the position L , T_{in} is the inflow fluid temperature.

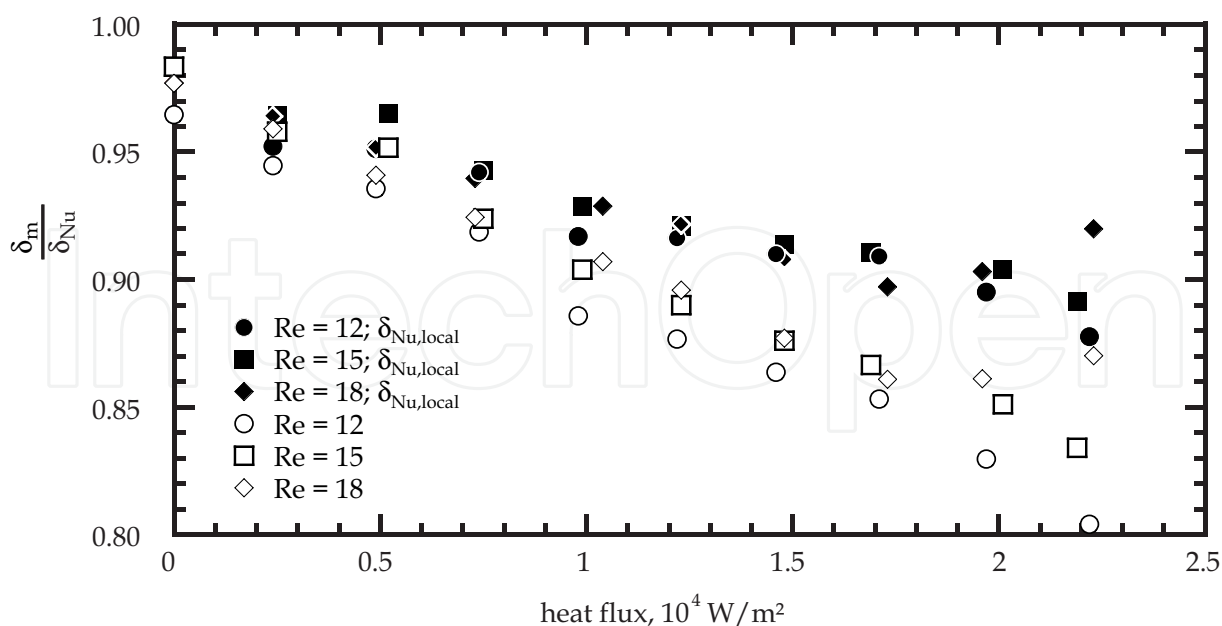


Fig. 10. Dimensionless film thickness, measured 60 mm downstream of the start of the heated section and averaged over the horizontal positions, as a function of heat flux, open symbols divided by Nusselt film thickness at the inflow temperature, filled symbols divided by local Nusselt film thickness. (Lel et al., 2008).

$$U_{TC} = \left| \frac{d\sigma}{dT} \right| \frac{\Delta T_z \delta_{res}}{\eta l_z}, \tag{11}$$

where ΔT_z is the characteristic temperature drop along l_z . Contrary to the model suggested in (Bohn & Davis, 1993) l_z is not the characteristic length scale but equal to one half of the distance between two structures as determined in experiments:

$$l_z = \frac{\Lambda_0}{2}. \tag{12}$$

In analogy to (Ganchev, 1984) dry spots may appear in the film when the time required for thermal-capillary breakdown in the residual layer and the period between the passing of two consecutive wave crests are of same order:

$$t_{TC} = t_w, \text{ thereby } t_{TC} = \frac{l_z}{U_{TC}}, \quad t_w = \frac{1}{f_w} = \frac{\lambda_w}{c_w}, \tag{13}$$

and f_w is the dominating frequency of large wave propagation, λ_w is the length of large waves and c_w is the phase velocity of large waves.

Fig. 12 shows the energy balance inside an infinitely small element in a film in the x-y plane. Neglecting the heat conduction in x direction and the convective heat transfer in y direction we obtain the equation:

$$\rho c_p u_x \frac{\partial T}{\partial x} = \lambda \frac{\partial^2 T}{\partial y^2} = -\frac{\partial \dot{q}''}{\partial y}. \tag{14}$$

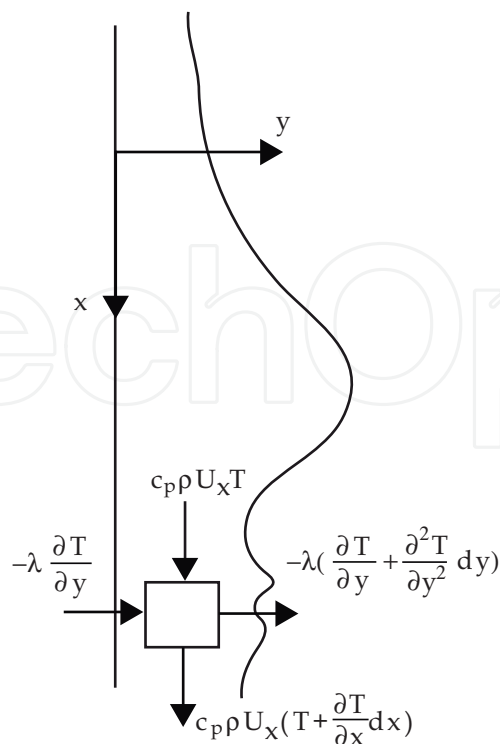


Fig. 12. Energy balance in the residual layer (Lel et al., 2007a)

Approximating this equation by a finite differential equation the typical temperature drop over $l_x \equiv 0.9\lambda_w$ can be determined:

$$\Delta T_x = \frac{\dot{q}_w''}{\delta_{res}} \frac{0.9\lambda_w}{\rho c_p U_{res}}, \quad (15)$$

Where \dot{q}_w'' is the heat flux at the wall, U_{res} is the average liquid velocity in the residual layer, ρ is the liquid density and c_p is the specific heat. The remaining ten percent of l_x correspond to the length of the wave front. The material properties are taken at inflow temperatures. From the thermographic pictures as presented in Fig. 7.c.1, the temperature difference in x and y direction can be evaluated. Thereby a proportionality can be determined.

$$\Delta T_z = k \cdot \Delta T_x. \quad (16)$$

As for current data the constant of proportionality is in the range between $1 < k < 5$. For further considerations a value of $k = 3$ was assumed.

$$\Delta T_z = 3\Delta T_x. \quad (17)$$

Now, substituting expressions (16) and (15) into (11), we obtain:

$$U_{TC} = \left| \frac{d\sigma}{dT} \right| \frac{1}{\eta} \frac{\dot{q}_w''}{l_z} \frac{0.9\lambda_w}{\rho c_p U_{res}} \frac{1}{3} \quad (18)$$

and (18) into (13):

$$\frac{1}{l_z} \left| \frac{d\sigma}{dT} \right| \frac{1}{\eta} \frac{\dot{q}_w''}{l_z} \frac{0.9\lambda_w}{\rho c_p U_{res}} \frac{1}{3} = \frac{c_w}{\lambda_w}. \quad (19)$$

Solving Eq. (19) for \dot{q}_w'' :

$$\dot{q}_w'' = \frac{1}{0.9} \frac{c_w}{\lambda_w^2} \frac{\rho c_p U_{res}}{\left| \frac{d\sigma}{dT} \right|} \frac{\eta l_z^2}{3} = \frac{1}{0.9} \frac{f_w^2}{c_w} \frac{\rho c_p U_{res}}{\left| \frac{d\sigma}{dT} \right|} \eta \frac{\Lambda_0^2}{4} \frac{1}{3}. \quad (20)$$

According to expression (20) the critical heat flux depends on the liquid properties, the frequency of large waves and the typical transverse size of regular structures. If the following dimensionless numbers are used:

$$Ma_q = \frac{\dot{q}_w'' \left| \frac{d\sigma}{dT} \right| \left(\frac{v^2}{g} \right)^{\frac{2}{3}}}{\lambda \rho v^2}, \quad Pr = \frac{v}{a} \quad \text{and} \quad K_\Lambda = \left(\frac{f_w \Lambda_0}{(vg)^{\frac{1}{3}}} \right)^2. \quad (21)$$

Equation (21) can be presented in the form:

$$\frac{Ma_q}{Pr K_\Lambda} = \frac{1}{0.9} \frac{U_{res}}{c_w} \frac{1}{4} \frac{1}{3} = \frac{1}{10.8} \frac{U_{res}}{c_w}. \quad (22)$$

Therefore, in Fig. 13 the experimental data for the dimensionless critical heat flux (Ma_q/PrK_Λ) are presented as a function of the Reynolds number. Only data which were obtained on excited falling films (with the help of the loud speaker) were used, allowing to keep the major frequency f_w at a constant value. As can be seen Eq. (22) depends on the relation between the mean velocity of the residual layer and the mean velocity of large waves. In the literature many different analytical and empirical equations can be found for these velocities as functions of the Reynolds number. For example in (Brauner & Maron, 1983) a physical model for the falling film is presented. In this case the ratio is constant:

$$\frac{U_{res}}{c_w} = 0.091. \tag{23}$$

Therefore the combination of dimensionless parameters from (22) is constant, too:

$$\frac{Ma_q}{PrK_\Lambda} = 8.43 \times 10^{-3}. \tag{24}$$

Equation (24) is in the same order for the dimensionless critical heat flux as the experimental data, but the trend of the latter has a different inclination, see Fig. 13.

In (Al-Sibai, 2004) the same silicone oils were used as in the current experiments. Therefore a better comparability could be given for dependencies from (Al-Sibai, 2004) as for other correlations from literature. Since the thickness of the residual layer is relatively small the Nusselt formula for laminar flow can be used:

$$U_{res} = \frac{g\delta_{res}^2}{3\nu}. \tag{25}$$

In (Al-Sibai, 2004) an equation for the residual layer thickness can be found:

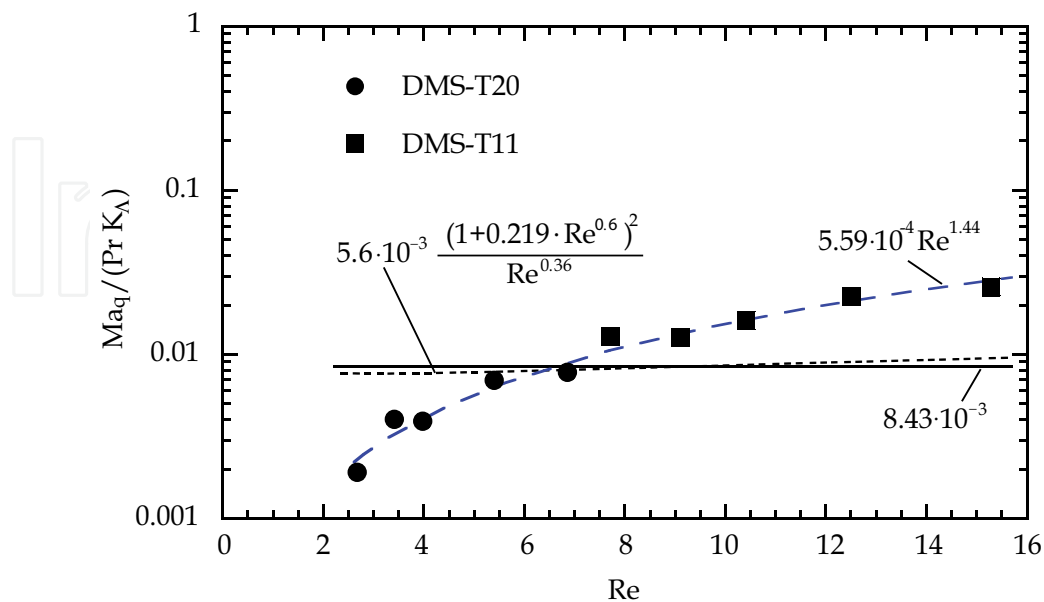


Fig. 13. The dependence of dimensionless parameter $Ma_q/(PrK_\Lambda)$ versus Reynolds-number. Points experimental data (Lel et al., 2007a)

$$\delta_{\text{res}} = \left(1 + 0.219\text{Re}^{0.6}\right) \left(\frac{v^2}{g}\right)^{\frac{1}{3}}. \quad (26)$$

Substituting (26) into (25):

$$U_{\text{res}} = \frac{1}{3} g^{\frac{1}{3}} v^{\frac{1}{3}} \left(1 + 0.219\text{Re}^{0.6}\right)^2 \quad (27)$$

and another equation from (Al-Sibai, 2004) giving the velocity of large waves against the Reynolds number:

$$c_w = 5.516 g^{\frac{1}{3}} v^{\frac{1}{3}} \text{Re}^{0.36}. \quad (28)$$

From Eq. (22) the following non-dimensional expression can be derived with substitutions (27) and (28):

$$\frac{\text{Ma}_q}{\text{Pr}K_\Lambda} = 5.6 \times 10^{-3} \frac{\left(1 + 0.219\text{Re}^{0.6}\right)^2}{\text{Re}^{0.36}}. \quad (29)$$

The comparison of dependence (29) with experimental data gives a good agreement in the order of magnitude but a difference in the inclination, see Fig. 13. For a Reynolds number range $\text{Re} < 3$ the dimensionless parameter $(\text{Ma}_q/\text{Pr}K_\Lambda)$ according to Eq. (29) even decreases, but the experimental data show another tendency.

This disagreement between experimental data and theory can be ascribed to the uncertainty of the proportionality factor in Eq. (16) as describes above.

As can be seen from (29):

$$\text{Ma}_q = f(\text{Re}, \text{Pr}, K_\Lambda). \quad (30)$$

This approximation found from experimental data analysis is:

$$\text{Ma}_q = 5.59 \times 10^{-4} \text{Re}^{1.44} \text{Pr} K_\Lambda. \quad (31)$$

In order to verify and consolidate this theory the range of Reynolds number should be increased. An elongating of heat section will allow the observation of further development of regular structures.

For the experiments without activated loud speaker the wavelength has to be determined by measuring the oscillations of the film surface and using the major frequency for the parameter K_Λ .

A comparison of experimental data with other dependencies from the literature is shown in the next part.

4.2 Comparing of experimental data with other approaches

In this part different approaches for the determination of the critical dimensionless heat flux are presented and compared with experimental data.

Experimental data for laminar-wavy and turbulent films were described in (Gimbutis, 1988) by the following empirical dependencies:

$$Ma_q = 0.522Re^{0.4} \left(1 + 0.12 \left(\frac{Re}{250} \right)^{4.5} \right)^{0.5} \quad \text{for } L \leq 1 \text{ m.} \quad (32)$$

For $100 < Re < 200$ in (Gimbutis, 1988) the scattering of data was up to 50 %, for $Re < 100$ no experimental data have been recorded. It can be seen in Fig. 14 that this dependence suggests lower values than the current experimental data. The difference can be explained by the fact that in (Gimbutis, 1988) the experimental data were obtained only for a water film flow with a relatively long heated section. In this case evaporation effects and thus a shift in the thermophysical properties could have appeared.

In (Kabov, 2000) the empirical dependence of the critical Marangoni number on the Reynolds number for a shorter heated section (6.5 mm length along the flow) for laminar waveless falling films was obtained:

$$Ma_q = 8.14Re^{0.98} . \quad (33)$$

In this case the length of the heated section is in the same order of magnitude as the thermal entry length (Kabov, 2000). Therefore this curve indicates higher values than our experimental data.

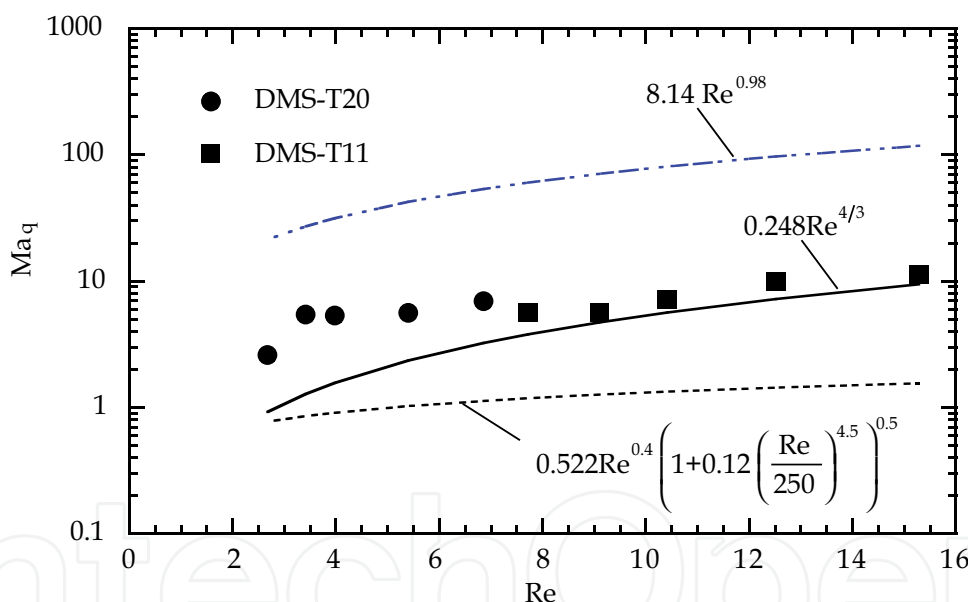


Fig. 14. The dependence of dimensionless parameter Ma_q versus the Reynolds-number. Points experimental data (Lel et al., 2007a)

It was shown in (Ito et al., 1995) that for the 2D case the modified critical Marangoni number is constant:

$$Ma_c = \frac{\dot{q}_w'' \left| \frac{d\sigma}{dT} \right|}{\lambda \rho U_s^2} = 0.23 . \quad (34)$$

With the film surface velocity based on Nusselt's film theory $U_s = (g/2\nu)\delta_m^2$, expression (34) can be transformed into:

$$\text{Ma}_q = 0.248\text{Re}^{4/3}. \quad (35)$$

It can be seen, that only dependence (35) is in the same order of magnitude as our experimental data.

Other dimensionless parameters for generalisation of experimental data were used in (Bohn & Davis, 1993) and (Zaitsev et al., 2004). In (Bohn & Davis, 1993) the data for dimensionless breakdown heat flux is approximated in the form:

$$\frac{\dot{q}_w'' \left| \frac{d\sigma}{dT} \right|}{\rho^{1/3} c_p \eta^{5/3} g^{2/3}} = 4.78 \times 10^5 \text{Re}^{1.43}. \quad (36)$$

With elementary transformations (36) can be transformed into:

$$\frac{\text{Ma}_q}{\text{Pr}} = 4.78 \times 10^5 \text{Re}^{1.43}. \quad (37)$$

Fig. 15 shows that (37) again leads to lower values than our experimental data. Here, as in case of Eq. (32), evaporation effects could have appeared, because this dependence was obtained for water and for a 30 % glycerol-water solution at a 2.5 m long test section for $\text{Re} > 959$.

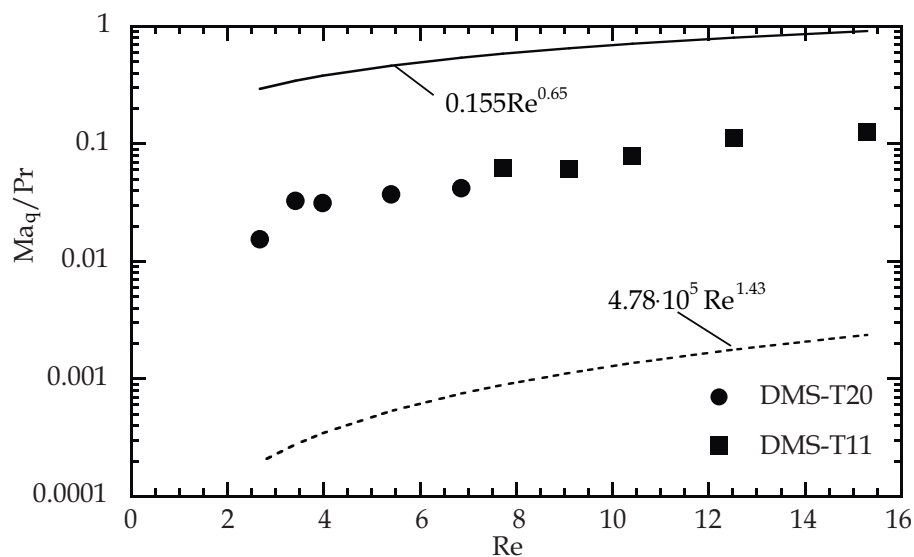


Fig. 15. The dependence of dimensionless parameter Ma_q/Pr versus the Reynolds-number. Points experimental data (Lel et al., 2007a)

A generalisation for water and an aqueous solution of alcohol is presented in (Zaitsev et al., 2004):

$$\frac{\text{Ma}_q}{\text{Pr}} = 0.155\text{Re}^{0.65}. \quad (38)$$

This correlation leads to results which exceed current data by more than one order of magnitude. This can be partially explained by the fact that dependence (38) was obtained for

stable dry spots, whereas the new data was recorded for the formation of local instable dry spots.

5. Thermal entry length

In this part experimental data for the thermal entry length with the correlation from the literature are compared and a new correlation, included dimensionless parameters incorporated several physical effects, is presented.

A comparison of experimental data for the thermal entry length with correlations for laminar flow by (Mitrovic, 1988) and (Nakoryakov & Grigorijewa, 1980), is shown in Fig. 16. Whereas for very low Reynolds numbers ($Re_0 < 3$) and heat fluxes the experimental data correlate satisfactorily with these dependencies, at larger Reynolds numbers and heat fluxes the experimental values lie under the ones obtained through correlations.

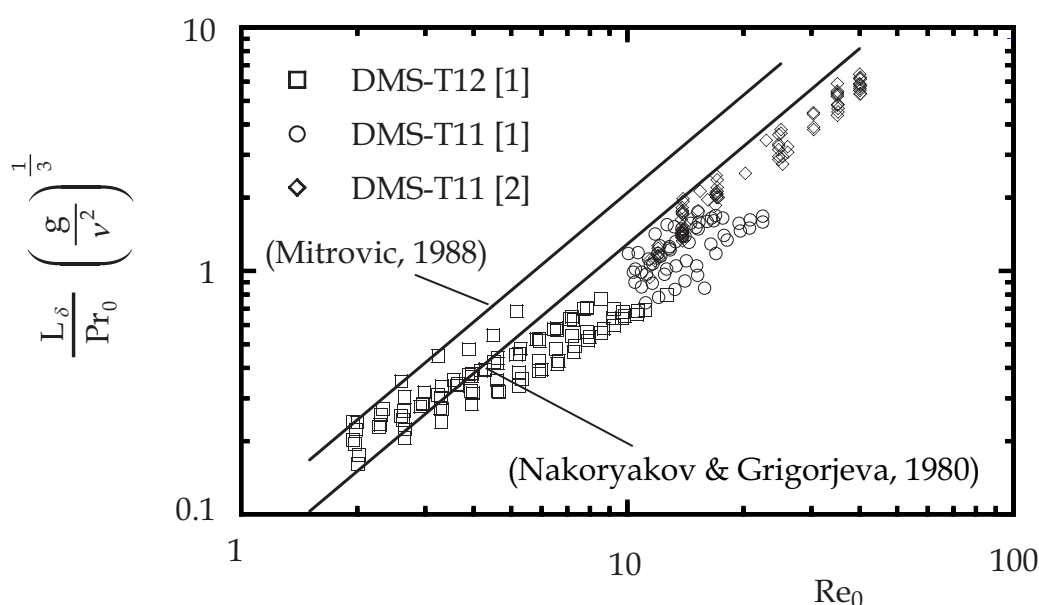


Fig. 16. Experimental data compared with solutions for smooth laminar falling films. [1] - experimental data by (Lel et al., 2007b); [2] - experimental data by (Lel et al., 2009).

Therefore, the experimental data were used in order to found a empirical dependency which describes the dimensionless entry length and attempts to incorporate several effects: i) the effect of nonlinear changing material properties due to temperature changes and the effects of ii) surface tension and iii) waves:

$$L_\delta = aRe_0^b Pr_0 Ka_0^{0.0606} \left(\frac{Pr_0}{Pr_w} \right)^{-0.29} \left(\frac{v^2}{g} \right)^{\frac{1}{3}} \tag{39}$$

$$\left. \begin{aligned} a &= 0.8367 \\ b &= 0.718 \end{aligned} \right\} \text{for } Re < 8$$

$$\left. \begin{aligned} a &= 0.022 \\ b &= 1.36 \end{aligned} \right\} \text{for } Re > 8$$

In Fig. 17 the comparison of experimental data with a correlation for $100 < Pr_0 < 180$ and $2 < Re_0 < 40$ is presented.

Here it is significant, that the differences of Eq. (1) and Eq. (39) are the additional terms involving Pr_0/Pr_W and the Kapitza number $Ka_0 = (\sigma^3 \rho / g \eta^4)$.

(Brauer, 1956) found that the Kapitza number has an influence on the development of the waves at the film surface. He defined the point of instability $Re_i = 0.72 Ka_0^{1/10}$, at which sinusoidal waves become unstable. Therefore, the Kapitza number has also to be implemented into correlations (39).

The relation Pr_0/Pr_W between the Prandtl number at the inflow and at the wall temperature has to be added into the dependence, in order to take into account the dependency of the viscosity of the fluid on the temperature.

The effect of the decrease of the thermal entry length flux because of Marangoni convection, described in (Kabov et al., 1996), is subject to debate. We assume that in this case the influence of the waves on the thermal entry length play a dominant role. This question stays unsettled and should be investigated in future.

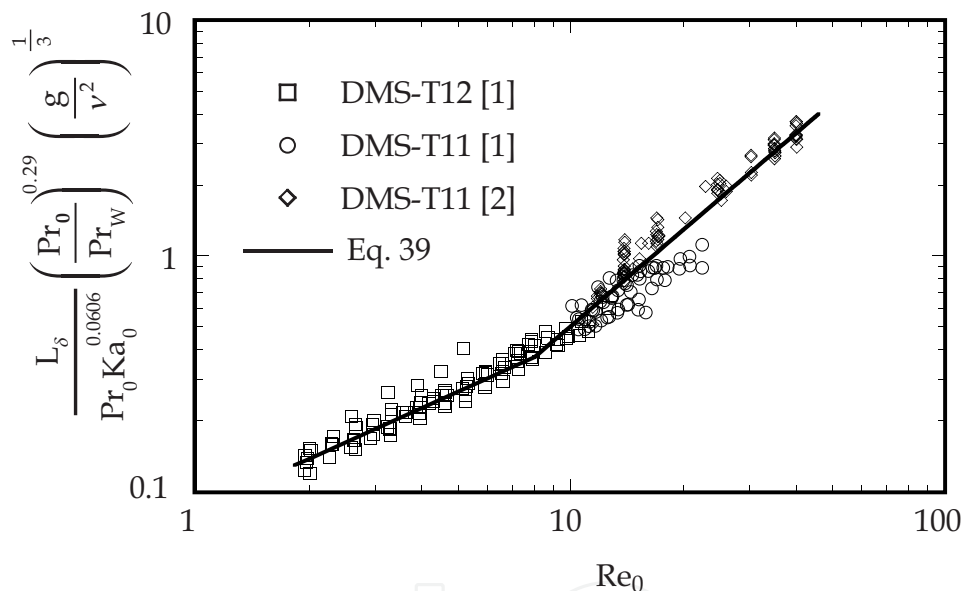


Fig. 17. Comparison of correlation (5) for thermal entry length for laminar wavy films with the experimental data. [1] - experimental data by (Lel et al., 2007b); [2] - experimental data by (Lel et al., 2009).

6. Conclusion

The results of the experimental investigation of different physical effects of heat and mass transfer in falling films were discussed in this chapter.

At first the visualization of quasi-regular metastable structures within the residual layer between large waves of laminar-wavy falling films were presented. To obtain a relation between the surface temperature and film thickness fields, infrared thermography and the chromatic confocal imaging technique were used.

By comparing the temperature and film thickness fields, the assumption of the thermo-capillary nature (Marangoni effect) of regular structures within the residual layer has been

confirmed. An increase in local surface temperature leads to a decrease in local film thickness. The evolution of the regular structure's "head" between two large parabolic shaped waves over time was presented.

The decrease of the mean film thickness could be explained by a reduction of the viscosity and a cross flow into the faster moving large waves. Both effects cause a higher film velocity.

The results obtained are important for the investigation of the dependency between wave characteristics and local heat transfer, the conditions of "dry spot" appearance and the development of crisis modes in laminar-wavy falling films.

A model of thermal-capillary breakdown of a liquid film and dry spot formation is suggested on the basis of a simplified force balance considering thermal-capillary forces in the residual layer. It is shown that the critical heat flux depends on half the distance between two hot structures, because the fluid within the residual layer is transferred from hot structures to the cold areas in between them. It also depends on the main frequency of large waves, the Prandtl number, the heat conductivity, the liquid density and the change in surface tension in dependence on temperature. The model is also presented in a dimensionless form.

The investigations of the thermal entry length of laminar wavy falling films by means of infrared thermography are shown. Good qualitative agreement with previous works on laminar and laminar wavy film flow was found at low Reynolds numbers. However, with increasing Reynolds numbers and heat fluxes, these correlations describe the thermal entry length inadequately. The correlation established for laminar flow was extended in order to include the effect of temperature-dependent non-linear material properties as well as for the effects of surface tension and waves.

7. Acknowledgements

This work was financially supported by the "Deutsche Forschungsgemeinschaft" (DFG KN 764/3-1). The authors thank the student coworkers and colleagues A. Kellermann, Dr. H. Stadler, Dr. G. Dietze, M. Baltzer, Dr. F. Al-Sibai, M. Allekotte for the help in the preparation of this chapter.

8. References

- Adomeit, P. & Renz, U. (2000). Hydrodynamics of three-dimensional waves in laminar falling films, *Int J Mult Flow*, Vol. 26, pp. 1183-1208
- Alekseenko, S.V.; Nakoryakov, V.E. & Pokusaev, B.G. (1994). *Wave flow of liquid films*, Fukano, T. (Ed.), p. 313, Begell House, Inc., New York
- Al-Sibai, F. (2004). Experimentelle Untersuchung der Strömungscharakteristik und der Wärmeübertragung bei welligen Rieselfilmen. *Thesis of Dr.-Ing. Degree*, Lehrstuhl für Wärme- und Stoffübertragung, RWTH Aachen
- Al-Sibai, F.; Leefken, A.; Lel, V.V. & Renz, U. (2003). Measurement of transport phenomena in thin wavy film. *Fortschritt-Berichte VDI 817 Verfahrenstechnik Reihe 3*, pp. 1-15

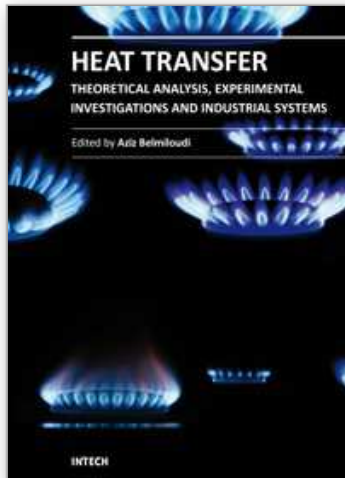
- Bohn, M.S. & Davis, S.H. (1993). Thermo-capillary breakdown of falling liquid film at high Reynolds number. *Int JHeat Mass Transf*, Vol. 7, pp. 1875-1881
- Bettray, W. (2002). FTIR measurements of spectral transmissivity for layers of silicone fluids with different thicknesses, *Technical Report of the Institute for Organic Chemistry at the RWTH Aachen University*, Germany
- Brauer, H. (1956). Strömung und Wärmeübergang bei Rieselfilmen, *VDI Forschungsheft 457*
- Brauner, N. & Maron, D.M. (1983). Modeling of wavy flow in inclined thin films. *Chem Eng Sci*, Vol 38, No. 5, pp. 775-788
- Chinnov, E.A. & Kabov, O.A. (2003). Jet formation in gravitational flow of a heated wavy liquid film, *JAppl Mech Tech Phys*, Vol. 44, No. 5, pp. 708-715
- Cohen-Sabban, J.; Crepin, P.-J. & Gaillard-Groleas, J. (2001). Quasi confocal extended field surface sensing, *Processing of Optical Metrology for the Semicon*, Optical and Data Storage Industries SPIE's 46th Annual Meeting, San Diego, August 2-3, CA, USA
- Ganchev, B.G. (1984). Hydrodynamic and heat transfer processes at downflows of film and two-phase gas-liquid flows (in Russian), *Thesis of Doctor's Degree in Phys-Math. Sci.*, Moscow
- Gimbutis, G. (1988). *Heat transfer at gravitation flow of a liquid film* (in Russian), *Mokslas*, Vilnius
- Ito, A.; Masunaga, N. & Baba, K. (1995). Marangoni effects on wave structure and liquid film breakdown along a heated vertical tube, In: *Advances in multiphase flow*, Serizawa, A.; Fukano, T.; Bataille, J. (Ed.), pp. 255-265, Elsevier, Amsterdam
- Kabov, O.A. (2000). Breakdown of a liquid film flowing over the surface with a local heat source. *Thermophys Aeromech*, Vol. 7, No.4, pp. 513-520
- Kabov, O.A. & Chinnov, E.A. (1998). Hydrodynamics and heat transfer in evaporating thin liquid layer flowing on surface with local heat source. In: *Proceedings of 11th international heat transfer conference*, Vol. 2, pp. 273-278, Kyondju, Korea, August 23-28
- Kabov, O.A.; Chinnov, E.A. & Legros, J.C. (2004). Three-dimensional deformations in non-uniformly heated falling liquid film at small and moderate Reynolds numbers, In: *2nd International Berlin Workshop—IBW2 on Transport Phenomena with Moving Boundaries*, Schindler, F.-P. (Ed.), pp. 62-80, Düsseldorf: VDI Verlag, VDI Reihe 3, No. 817, 9-10 October, Germany
- Kabov, O.A.; Diatlov A.V. & Marchuk, I.V. (1995). Heat transfer from a vertical heat source to falling liquid film, In: *G.P. Celata and R.K. Shah, Editors, Proceeding of First Internat. Symp. on Two-Phase Flow Modeling and Experimentation*, Vol.1, pp. 203-210, Rome, Italy, 1996
- Kabov, O.A.; Marchuk, I. V. & Chupin, V.M. (1996). Thermal imaging study of the liquid film flowing on vertical surface with local heat source. *Russ. J Eng. Thermophys*, Vol. 6, No. 2, pp. 104-138
- Kabov, O.A.; Legros, J.C.; Marchuk IV & Scheid, B. (2001). Deformation of free surface in a moving locally-heated thin liquid layer. *Fluid Dyn*, Vol. 36, No. 3, pp. 521-528
- Klein, D.; Hetsroni, G. & Mosyak, A. (2005). Heat transfer characteristics of water and APG surfactant solution slow in a micro-channel heat sink, *Int JMult Flow*, Vol. 31, No. 4, pp.393-415

- Lel, V.V.; Al-Sibai, F.; Leefken, A. & Renz, U. (2005). Local thickness and wave velocity measurement of wavy falling liquid films with chromatic confocal imaging method and a fluorescence intensity technique, *Exp Fluids*, Vol. 39, pp. 856-864
- Lel, V.V.; Al-Sibai, F. & Kneer, R. (2009). Thermal entry length and heat transfer phenomena in laminar wavy falling films, *Microgravity Sci. Technol*, Vol. 21 (Suppl 1), pp. 215-220
- Lel, V.V.; Dietze, G.F.; Stadler, H.; Al-Sibai, F. & Kneer, R. (2007b). Investigation of the Thermal Entry Length in Laminar Wavy Falling Films, *Microgravity sci. technol.*, Vol. XIX-3/4, pp. 66-68
- Lel, V.V.; Kellermann, A.; Dietze, G.; Kneer, R. & Pavlenko, A.N. (2008). Investigations of the Marangoni effect on the regular structures in heated wavy liquid films, *Exp Fluids*, Vol.44, pp. 341-354
- Lel, V.V.; Stadler, H.; Pavlenko, A. & Kneer, R. (2007a). Evolution of metastable quasi-regular structures in heated wavy liquid films, *JHeat Mass Transf*, Vol. 43, No. 11, pp. 1121-1132
- Ludviksson, V. & Lightfoot, E.N. (1968). Hydrodynamic stability of Marangoni films, *AICHE J* Vol. 14, No. 4, pp. 620-626
- Mayerlen, W. & Tacke, M. (2002). Measurements of spectral reflectance of silicone fluids, *Technical report of FGAN-FOM*, Forschungsinstitut für Optronik und Mustererkennung, Germany
- Mitrović, J. (1988). Der Wärmeaustausch am Berieselungskühler. *Brennstoff-Wärme-Kraft*, Vol. 40, No. 6, pp. 243-249
- Nakoryakov V.E. & Grigorjeva, N.I. (1980). Calculation of heat and mass transfer in nonisothermal absorption on the initial portion of downflowing films. *Theoretical Foundations of Chemical Engineering*, Vol. 14, pp. 305-309
- Pavlenko, A.N. & Lel, V.V. (1997). Heat transfer and crisis phenomena in falling films of cryogenic liquid, *Russ JEng Thermophys*, Vol. 3-4, No. 7, pp. 177-210
- Pavlenko, A.N.; Lel, V.V.; Serov, A.F.; Nazarov, A.D. & Matsekh, A.M. (2002). Wave amplitude growth and heat transfer in falling intensively evaporating liquid film, *J Eng Thermophys*, Vol. 11, No. 1, pp. 7-43
- Ruyer-Quil, C.; Scheid, B.; Kalliadasis, S.; Velarde, M.G. & Zeytounian, R.K. (2005). Thermocapillary long waves in a liquid film flow. Part 1. Low dimensional formulation, *JFluid Mech*, Vol. 538, pp. 199-222
- Scheid, B.; Ruyer-Quil, C.; Kalliadasis, S.; Velarde, M.G. & Zeytounian, R.K. (2005). Thermocapillary long waves in a liquid film flow. Part 2. Linear stability and nonlinear waves, *JFluid Mech*, Vol. 538, pp. 223-244
- Scheid, B.; Ruyer-Quil, C. & Manneville, P. (2006). Wave patterns in film flows. Modeling and three-dimensional waves, *JFluid Mech*, Vol. 562, pp. 183-222
- Slattery, J. & Stuckey, E.L.; *Trans R Soc Can Sect*, Vol. XXVI, pp. 131
- Trevelyan, P.M.J. & Kalliadasis, S. (2004). Wave dynamics on a thin liquid film falling down a heated wall, *JEng Maths*, Vol. 50, pp. 177-208
- Yüksel, M.K. & Schlünder, E.U. (1988). Wärme- und Stoffübertragung bei der Nichtisothermen Rieselfilmabsorption, *Wärme- und Stoffübertragung*, Vol. 22, pp. 209-218

Zaitsev, D.V.; Kabov, O.A.; Cheverda, V.V. & Bufetov, N.S. (2004). The effect of wave formation and wetting angle on the thermocapillary breakdown of a falling liquid film. *High Temperature*, Vol. 42, No. 3, pp. 450-456

IntechOpen

IntechOpen



Heat Transfer - Theoretical Analysis, Experimental Investigations and Industrial Systems

Edited by Prof. Aziz Belmiloudi

ISBN 978-953-307-226-5

Hard cover, 654 pages

Publisher InTech

Published online 28, January, 2011

Published in print edition January, 2011

Over the past few decades there has been a prolific increase in research and development in area of heat transfer, heat exchangers and their associated technologies. This book is a collection of current research in the above mentioned areas and discusses experimental, theoretical and calculation approaches and industrial utilizations with modern ideas and methods to study heat transfer for single and multiphase systems. The topics considered include various basic concepts of heat transfer, the fundamental modes of heat transfer (namely conduction, convection and radiation), thermophysical properties, condensation, boiling, freezing, innovative experiments, measurement analysis, theoretical models and simulations, with many real-world problems and important modern applications. The book is divided in four sections : "Heat Transfer in Micro Systems", "Boiling, Freezing and Condensation Heat Transfer", "Heat Transfer and its Assessment", "Heat Transfer Calculations", and each section discusses a wide variety of techniques, methods and applications in accordance with the subjects. The combination of theoretical and experimental investigations with many important practical applications of current interest will make this book of interest to researchers, scientists, engineers and graduate students, who make use of experimental and theoretical investigations, assessment and enhancement techniques in this multidisciplinary field as well as to researchers in mathematical modelling, computer simulations and information sciences, who make use of experimental and theoretical investigations as a means of critical assessment of models and results derived from advanced numerical simulations and improvement of the developed models and numerical methods.

How to reference

In order to correctly reference this scholarly work, feel free to copy and paste the following:

Viacheslav V. Lel and Reinhold Kneer (2011). Heat Transfer Phenomena in Laminar Wavy Falling Films: Thermal Entry Length, Thermal-Capillary Metastable Structures, Thermal-Capillary Breakdown, Heat Transfer - Theoretical Analysis, Experimental Investigations and Industrial Systems, Prof. Aziz Belmiloudi (Ed.), ISBN: 978-953-307-226-5, InTech, Available from: <http://www.intechopen.com/books/heat-transfer-theoretical-analysis-experimental-investigations-and-industrial-systems/heat-transfer-phenomena-in-laminar-wavy-falling-films-thermal-entry-length-thermal-capillary-metasta>

INTECH
open science | open minds

InTech Europe

University Campus STeP Ri

InTech China

Unit 405, Office Block, Hotel Equatorial Shanghai

www.intechopen.com

Slavka Krautzeka 83/A
51000 Rijeka, Croatia
Phone: +385 (51) 770 447
Fax: +385 (51) 686 166
www.intechopen.com

No.65, Yan An Road (West), Shanghai, 200040, China
中国上海市延安西路65号上海国际贵都大饭店办公楼405单元
Phone: +86-21-62489820
Fax: +86-21-62489821

IntechOpen

IntechOpen

© 2011 The Author(s). Licensee IntechOpen. This chapter is distributed under the terms of the [Creative Commons Attribution-NonCommercial-ShareAlike-3.0 License](#), which permits use, distribution and reproduction for non-commercial purposes, provided the original is properly cited and derivative works building on this content are distributed under the same license.

IntechOpen

IntechOpen